

# **STUDY OF THE EFFECTIVENESS OF TANTALUM-RUTHENIUM AS A HYDROGEN SENSING MATERIAL**

## **Bachelor Thesis**

To obtain the degree of

**Bachelor of Science**  
in Applied Physics,

at the Delft University of Technology,  
to be defended on Thursday August 19, 2021 at 15:00 PM.

Student number:	4690575	
Daily supervisor:	Dr. ir. L.J. Bannenberg	TNW/RST
Defense committee:	Dr. ir. L.J. Bannenberg	TNW/RST
	Prof. dr. B. Dam	TNW/ChemE

by

**Nathan VAN BEUGEN**

Delft, Netherlands  
August, 2021



# CONTENTS

<b>Abstract</b>	<b>1</b>
<b>1 Introduction</b>	<b>3</b>
<b>2 Theory</b>	<b>5</b>
2.1 The ideal hydrogen sensor . . . . .	5
2.2 Thermodynamics of thin films . . . . .	6
2.3 Effect of Hydrogen on optical properties . . . . .	8
2.4 Effect of Ru doping on the structure of Ta . . . . .	8
2.5 X-ray diffraction. . . . .	9
<b>3 Experimental methods</b>	<b>11</b>
3.1 Sample preparation . . . . .	11
3.2 Hydrogenography measurements . . . . .	12
3.3 Response time measurements . . . . .	12
3.4 Ex situ XRD measurements . . . . .	13
3.4.1 Bragg-Brentano diffractograms . . . . .	13
3.4.2 Rocking Curves . . . . .	14
3.5 In situ XRD measurements . . . . .	14
3.6 In situ XRR measurements . . . . .	14
<b>4 Results</b>	<b>17</b>
4.1 Optical response of the sensing material . . . . .	17
4.2 Structural measurements . . . . .	22
<b>5 Discussion</b>	<b>27</b>
<b>6 Conclusion</b>	<b>29</b>
<b>Appendix</b>	<b>31</b>
<b>References</b>	<b>35</b>



# ABSTRACT

As hydrogen can make an important contribution in the energy transition, its detection is necessary for safe application. Optical hydrogen sensors are a promising alternative to conventional hydrogen sensors as they are smaller, less expensive and safer. These sensors show a change in optical transmission upon exposure to hydrogen, allowing the partial hydrogen pressure to be probed. The optical response and the structural properties of Pd capped  $\text{Ta}_{1-x}\text{Ru}_x$  thin films are studied. A sensing range of 7 orders of magnitude in partial hydrogen pressure is observed, with a significant change in optical transmission upon hydrogenation. Exposure to hydrogen results in a phase transition of the Pd capping layer, leading to the hysteresis in the optical response of the sensor. This phase transition can be suppressed by alloying the capping layer. A sub-second response time is observed for large hydrogen pressures, which can be improved significantly using an additional PTFE layer. Phase transitions of the  $\text{Ta}_{1-x}\text{Ru}_x$  layer are suppressed by the nanoconfinement of the sensing layer, and a solid solution is formed. The sensing range of  $\text{Ta}_{1-x}\text{Ru}_x$  can be tuned by alloying Ta with Ru, resulting in a shift of the sensing range to higher hydrogen pressures. Implementing the suggested improvements would result in a hydrogen sensor with a sub-second response time and a tuneable sensing range of 7 orders of magnitude free of any hysteresis, proving  $\text{Ta}_{1-x}\text{Ru}_x$  to be an effective material for hydrogen sensing.



# 1

## INTRODUCTION

Hydrogen plays a significant role in the transition of an energy system based of fossil fuels to renewable energies. It can contribute to the CO<sub>2</sub> reduction in heavy transport or mobility, and its transport and storage is even possible with the existing infrastructure for natural gas [1].

Fast and reliable detection of hydrogen is necessary for safe applications, as it is highly flammable in air. Conventional hydrogen detection is done using catalytic resistors or electrochemical devices. As these sensors can pose a explosion hazard, have a limited sensing range and require regular calibration, optical hydrogen sensors are a viable alternative [2].

Optical hydrogen sensors are promising as they are relatively small, inexpensive and more safe, as they do not require electric currents for sensing. These sensors show a change in optical transmission upon exposure to hydrogen. A change in partial H<sub>2</sub> pressure in the environment changes the hydrogenation of the metal, resulting in an expansion of the material and a change of the dielectric function , changing the optical transmission. By measuring the optical response of the sensors, the partial H<sub>2</sub> pressure thus can be determined.

Sensing materials for optical hydrogen sensors need to satisfy requirements such as a no dependency on pressure history, a large sensing range, and a fast response. Tantalum already has already proven to be usable as a sensing material with a sensing range of 7 orders of magnitude in  $P_{H_2}$ , no hysteresis and a response time under half a minute [3]. Alloying of Ta with Pd results in an optical hydrogen sensor with a sensing range of 7 orders of magnitude, no hysteresis and an even faster sub-second response time [3].

The goal of this report is to study the effectiveness of Ta<sub>1-x</sub>Ru<sub>x</sub> as a material for hydrogen sensing. To find a sensing material with an even larger or different sensing range, other operating temperature or faster response times, we alloy Ta with Ru. As the atomic radius of Ru is smaller than Pd, alloying Ta with Ru could result in a sensor suitable at

even higher partial  $H_2$  pressures than  $Ta_{1-x}Pd_x$ .

The effect of Ru doping on the structure of Ta and its effect on the hydrogenation of the material is studied. We will note that  $Ta_{1-x}Ru_x$  is formed as a solid solution and in a single phase and that phase transitions, known to cause hysteresis, upon hydrogenation are suppressed by nanoconfinement of the material. Hydrogen cycling leads to settling of the material, resulting in a deviation from Vegard's law.

The optical response of  $Ta_{1-x}Ru_x$  studied along with the the change in optical contrast and sensitivity. A large sensing range of 7 orders of magnitude is noted for temperatures of  $T = 28 - 120^\circ C$ . The sensing material shows a response time under 15 seconds for  $P_{H_2} = 1.5 \cdot 10^2 - 2.0 \cdot 10^3$  and suggestions are made for a faster response.

# 2

## THEORY

Detection of hydrogen is possible using thin film metal hydride optical sensors. The optical transmission of these sensors change with the hydrogenation of the sensing layer resulting from a change of the partial  $H_2$  pressure to which they are exposed. The sensor studied consists of a optically transparent quartz substrate, a Ti adhesion layer, a  $Ta_{1-x}Ru_x$  sensing and a Pd capping layer. The Pd capping layer is responsible for breaking up the atomic bonds of  $H_2$ , while the hydrogenation of the  $Ta_{1-x}Ru_x$  sensing layer changes the optical transmission. Hydrogenation is the increase of hydrogen content in a material through the absorption of hydrogen atoms. The Pd capping layer moreover prevents oxidation and nitridation of the  $Ta_{1-x}Ru_x$  sensing layer. In the following sections the relevant physical mechanisms are studied and desirable sensor properties are translated into material properties.

### 2.1. THE IDEAL HYDROGEN SENSOR

We will study the effectiveness of  $Ta_{1-x}Ru_x$  as as sensing material for hydrogen sensing. As one can imagine, properties such as a large sensing range and a fast response time are desirable. As indicated in Table [2.1], such properties can be translated into several material properties of the thin film samples (adapted from Ref.[4]).

Table 2.1: Summary of several desirable properties of a sensor for effective hydrogen sensing, and how to achieve these properties in terms of material properties.

	<b>Achieved by</b>
<b>Large sensing range</b>	Large range of H <sub>2</sub> solubility within one phase Small $dx/dP_{H_2}$
<b>Large optical contrast</b>	Large $dx/dP_{H_2}$ Large change of dielectric function with hydrogen content Take wavelength where change in optical response is the largest
<b>No hysteresis</b>	No phase transition upon hydrogenation No stress-induced hysteresis
<b>Fast response time</b>	Thin sensing layer Apply surface coatings to lower activation energy
<b>High stability</b>	Low volumetric expansion Good adhesion between sensing layer and substrate

A large sensing range over multiple orders of magnitude in partial H<sub>2</sub> pressure is desired. This can be achieved by having a large amount of hydrogen that can be absorbed in the sensing layer. To have any change in optical properties throughout this whole pressure range, we want also want a small increase of hydrogen ( $x$ ) in the sensing material with an increase of partial pressure to ensure this.

This conflicts with the requirement of a large optical contrast; the total change in optical transmission throughout the pressure range. As the absorption of hydrogen changes the optical transmission (see Section [2.3]), a large increase of hydrogen content with an increase of partial pressure is thus desired for a large contrast. Other sensing materials indicate a wavelength-dependent optical contrast [3], the optical response is thus to be measured for a wavelength resulting in the largest contrast.

The sensor should not have any dependency on its pressure history. Section [2.2] discusses the mechanisms involved with hysteresis and the thermodynamics of thin films. To ensure a fast response time of the sensor we want a thin sensing layer, as this reduces the amount of hydrogen that needs to be absorbed/dissociated by the Pd capping layer. This is because the Pd capping layer is the limiting factor in response times for pure Ta thin films [5].

An adhesive Ti layer is used to attach the sensing layer to the substrate. As the sensing material expands with increasing hydrogen content, delamination of the films is prevented by a low volumetric expansion and the use of a Ti adhesion layer [4].

## 2.2. THERMODYNAMICS OF THIN FILMS

The use of Ta<sub>1-x</sub>Ru<sub>x</sub> as a thin film, as opposed to bulk, leads to a nanoconfinement of the material. Since expansion of a film in the  $x/y$  direction is not allowed, only a vertical expansion of the thin film is possible. This vertical expansion is due to the hydrogenation of the sensing layer, leading to an expansion of this layer to accommodate the hydrogen atoms. Because the thin film is attached to the substrate with an adhesive layer, large adhesive forces hold the expanding sensing layer to the substrate. This is called clamping, and it results in large stresses in the sensing layer, altering the thermodynamics of Ta<sub>1-x</sub>Ru<sub>x</sub>.

The phase diagram of  $Ta_{1-x}Ru_x$  (Figure [2.1]) contains several phases in the dopant concentration range of  $0.5 \leq x \leq 1$  in  $Ta_{1-x}Ru_x$  at  $T=28^\circ\text{C}$ . Clamping often reduces the critical temperature in thin films; the temperature above which multiple phases transition to the same phase. This could result in the transition from the Ta phase to RuTa, RuTa', RuTa'' not being made at all upon hydrogenation, which is necessary for a large range of hydrogen solubility in a single phase.

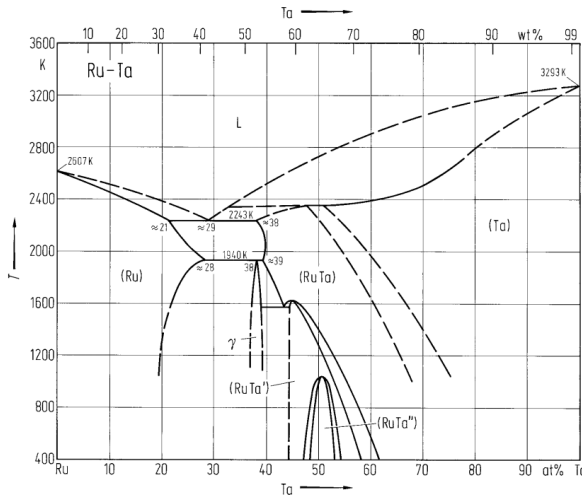


Figure 2.1: Phase diagram of Tantalum-Ruthenium [6], the dashed lines represent phases that may or may not occur at that temperature.

The dependency of an optical hydrogen sensor on pressure history, hysteresis, reveals itself in a difference in optical response for increasing and decreasing partial  $H_2$  pressures. Hysteresis can be caused by first order phase transitions [4], or elastic/plastic deformations of the sensor [7]. Plastic deformations are due to a large expansion of the sensing layer, causing large internal stresses due to clamping. These stresses can cause permanent deformations in the  $Ta_{1-x}Ru_x$  lattice such as the creation or movement of dislocations.

Elastic deformations can be explained using two mechanisms. It can be explained by a difference in lattice stress when the hydrogen content is increased or decreased. For hydrogen to be absorbed in the material, it needs to be accommodated between the atoms, creating additional stress in the lattice. An energy barrier thus needs to be overcome to achieve this, which is not present for the desorption of hydrogen.

A second explanation is the presence of multiple phases in the metal. The presence of these phases can vary depending on the hydrogen content of the metal. These phases introduce a different amount of stress into the lattice. This leads to a different amount of energy being required to (de)hydrogenate the metal, depending on the history of the material. For an optical response without hysteresis we thus want the alloy to be formed in a single phase, and no phase transition of  $Ta_{1-x}Ru_x$  upon hydrogenation. [7]

### 2.3. EFFECT OF HYDROGEN ON OPTICAL PROPERTIES

Palladium has been known to dissociate the hydrogen molecule easily; break the bonds between the two H atoms. As a H atom approaches the Pd surface, the molecule is held to the surface by Van der Waals forces [8]. Breaking up the hydrogen bond requires little or no energy for Pd surfaces [9]. After this dissociation, the hydrogen atoms are absorbed into the metal lattice.

In the metal lattice, the absorption of hydrogen has several effects: the already mentioned expansion of the lattice, but also a change in the optical transmission of the material. The law of Lambert-Beer relates material properties to the absorption of light which travels through it:

$$T(x, \lambda, z) = \frac{I(z)}{I_0} = e^{-\mu(x, \lambda)z} \quad (2.1)$$

Where  $T$  is the transmittance of the material; the thickness-dependent intensity  $I(z)$  relative to the initial intensity  $I_0$ . It is dependent on the thickness of the metal layer  $z$  and the attenuation coefficient  $\mu(x, \lambda)$ , which is a function of hydrogen concentration  $x$  and wavelength  $\lambda$ . When considering a two phase system, the attenuation coefficient is a weighted sum of their attenuation coefficients. For such a system, Eq.[2.1] can be rewritten as:

$$\ln\left(\frac{T(x, \lambda, z)}{T_0}\right) = -c(\lambda)\Delta xz \quad (2.2)$$

There thus is a linear relationship between  $\ln(T(x, \lambda, z)/T_0)$  and the hydrogen concentrations  $x$  in the material. The transmittance moreover is dependent on the layer thickness  $z$  and a wavelength-dependent constant  $c(\lambda)$ . This equation is used to model the optical transmission of solid solutions, although it is derived for two phase systems. Indeed, it has been found that Eq.[2.2] often is obeyed by systems in a single phase, such as Pd-capped Hf or Ta [4].

### 2.4. EFFECT OF RU DOPING ON THE STRUCTURE OF TA

The sensing layer  $\text{Ta}_{1-x}\text{Ru}_x$  has a Body Centered Cubic (BCC) unit cell for  $x=0$  [10]. Assuming no phase transitions happen upon increasing dopant concentration (Section [2.2]), the doping changes how atoms are arranged within the unit cell, as well as the size of the unit cell. It is possible that a solid solution is formed, where Ru atoms are incorporated into the metal lattice by replacing any Ta atom in the unit cell by Ru with a probability depending on dopant concentration. However, it is also possible that only a single atom of the unit cell is replaced.

For solid solutions an empirical relation often is observed for the change in lattice parameter upon alloying; Vegard's law [11]. It has been found that the lattice parameter for a solid solution is a weighted mean of the constituents of many alloys, e.g. for a solid solution of atom  $A$  and  $B$ :

$$a_{A_{1-x}B_x} = (1-x) \cdot a_A + x \cdot a_B \quad (2.3)$$

With  $x$  being the concentration of dopant  $B$ . This weighted mean is the result of the distortion of the metal lattice to incorporate the dopant.

## 2.5. X-RAY DIFFRACTION

Diffraction experiments are performed to study the change of the unit cell upon Ru doping and hydrogenation. In these experiments X-ray photons scatter off the electrons from the atoms in the material, resulting in a difference in wave vector between the incoming and scattered wave.

If we have a metal lattice with atoms separated by lattice vector  $\mathbf{R}$ , then these atoms are separated by a vector  $\mathbf{G}$  in reciprocal space, with the relation between these vectors given as  $\mathbf{G} \cdot \mathbf{R} = 2\pi n$  [12]. Assuming elastic scattering, constructive interference requires that the difference in wave vector of the incoming and scattering wave equals  $\mathbf{k}' - \mathbf{k} = \mathbf{G}$ : the Laue condition.

An equivalent statement can be derived using the Bragg formulation [13]; the scattered waves interfere constructively with each other if the difference in traveled distance results in a phase difference of  $\Delta\phi = 2\pi n$  (Figure [2.2]). With a distance  $d$  between the atomic layers, a wavelength  $\lambda$ , an angle  $\theta$  between the atomic planes and incoming wave and using geometry, Bragg's law can be derived:

$$n\lambda = 2d \sin(\theta) \quad (2.4)$$

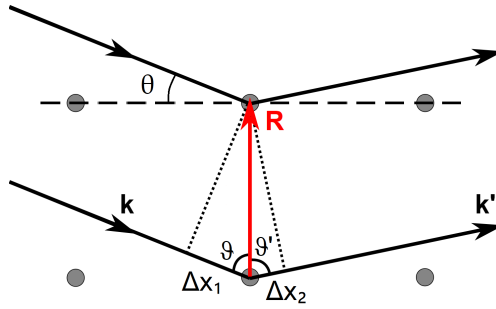


Figure 2.2: Scattering of the X-ray waves from a crystal lattice. The difference in traveled distance of  $\Delta x_1 + \Delta x_2$  results in a phase difference between the upper and lower scattered X-ray.

The constructive interference leads to the observation of a diffraction peak. The intensity of this peak is proportional to the absolute value squared of the amplitude of the scattered wave, which is proportional to the structure factor:

$$I \propto |S_{hkl}|^2 = \left| \sum_j f_j e^{i\mathbf{G}\mathbf{r}_j} \right|^2 \quad (2.5)$$

The structure factor  $S_{hkl}$  is due to atomic planes defined by the reciprocal lattice vector  $(hkl)$  and  $f_j$  is the complex scattering amplitude of the atom on location  $j$  in the unit cell. The vector  $\mathbf{G}$  is the difference between the incoming and outgoing wavevector  $\mathbf{k}$  and  $\mathbf{k}'$ , and  $\mathbf{r}_j$  is the location of atom  $j$  in the unit cell with respect to the reference lattice point [13]. For a BCC lattice the structure factor becomes:

$$S_{hkl} = f_{(0,0,0)} + f_{(\frac{1}{2}, \frac{1}{2}, \frac{1}{2})} \cdot e^{2\pi i(h \cdot \frac{1}{2}, k \cdot \frac{1}{2}, l \cdot \frac{1}{2})} = f_{(0,0,0)} + f_{(\frac{1}{2}, \frac{1}{2}, \frac{1}{2})} (-1)^{h+k+l} \quad (2.6)$$

If we study the diffraction peak due to the  $d_{110}$  spacing between atomic planes characterized by (110) and we would have a solid solution, the structure factor for  $x \leq 0.5$  would look like:

$$S_{110} = 2x \cdot f_{Ru} + 2(1 - x) \cdot f_{Ta} \quad (2.7)$$

Where the scattering amplitudes correspond to  $f_{Ta} = 67.51 + 5.48i$  and  $f_{Ru} = 44.08 + 3.18i$  for a source with  $\lambda = 0.154$  nm photons in diffraction experiments [14].

# 3

## EXPERIMENTAL METHODS

### 3.1. SAMPLE PREPARATION

The optical hydrogen sensor used (Figure [3.1a]) is 6 mm x 6 mm, and consists of a quartz substrate on which a 5 nm layer of Ti is sputtered as an adhesion layer for the sensing material  $Ta_{1-x}Ru_x$ . The  $Ta_{1-x}Ru_x$  sensing layer is 40 nm thick with  $0 \leq x \leq 0.5$  and the Pd capping layer 10 nm. Aside from these samples with a  $Ta_{1-x}Ru_x$  sensing layer, an additional sample is sputtered with  $Ta_{0.5}Pd_{0.5}$  instead of  $Ta_{1-x}Ru_x$ . On the use of this sample is elaborated in Section [3.2].

To achieve these thin films, a AJA1 sputtering system is used to sputter the samples in an Ar environment with a base pressure of 3  $\mu$ bar, a schematic of the setup used is illustrated in Figure [3.1b]. Typical deposition rates are 0.56  $\text{\AA}/s$  (100W DC) for Ti, 1.48  $\text{\AA}/s$  (100W DC) for Ta, 1.69  $\text{\AA}/s$  (50W DC) for Pd and 1.24  $\text{\AA}/s$  (100W DC) for Ru. Sputtering is a type of Physical Vapor Deposition (PVD) and is used to deposit materials onto a substrate. In this process, a target consisting of the material to be deposited, is impacted by energetic Ar ions which results in the ejection of substrate atoms. The Ar gas is ionized by applying a high voltage between the target and the substrate, this potential also accelerates the Ar ions onto the target. The vapor of ejected substrate atoms then condenses on the substrate, forming an atomic layer [15].

After sputtering, ex situ XRD measurements (Section [3.4]) are performed to validate the thickness of the layers. These indicate that the thickness of the Ti,  $Ta_{1-x}Ru_x$  and Pd layers are respectively  $5.17 \pm 0.56$ ,  $41.33 \pm 0.95$  and  $10.58 \pm 0.82$  nm. The deviations for all layers from their intended thickness are within 6%.

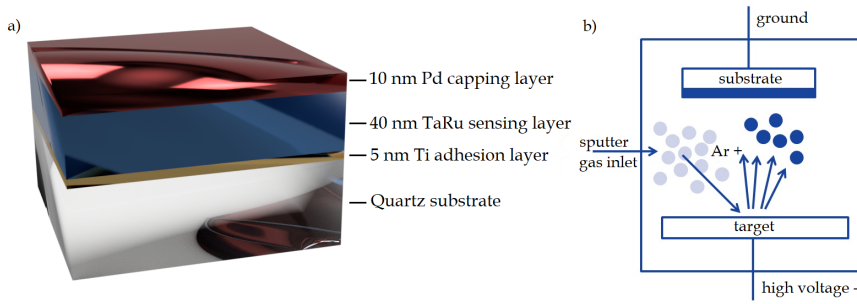


Figure 3.1: a) The sample used rendered schematically. Colors and dimensions not true to life. From top to bottom; the 10 nm Pd capping layer, the 40 nm  $\text{Ta}_{1-x}\text{Ru}_x$  sensing layer, a 5 nm Ti adhesion layer and the quartz substrate. b) Diagram of the DC sputtering system, image from [16]. The substrate used is quartz, and multiple targets of Pd, Ta, Ru, Ti are used to sputter the samples.

### 3.2. HYDROGENOGRAPHY MEASUREMENTS

The optical response of the samples to hydrogenation can be studied using hydrogenography measurements. In hydrogenography measurements, the change in optical transmission of samples is measured when varying the partial hydrogen pressure to which the samples are exposed. The samples are placed in an optically transparent and gas tight cell, in which they are exposed to a range of  $P_{\text{H}_2} = 1.0 \cdot 10^{-1} - 1.0 \cdot 10^6$  Pa, for an hour per pressure. The gas pressure in the cell is regulated by electronic inlet and outlet valves and a flow meter. The inlet valve is controlled by a MKS 250 forward Proportional-Integral-Differential (PID) system. The partial pressure range is achieved by using 3 different gas mixtures, see Table [3.1] for details.

The optical transmission of the samples is measured using a DFK 23UM021 USB color 1,280×960 camera from The Imaging Source with a  $\frac{1}{3}$  inch CMOS sensor. Four Philips GU5.3 Master LEDs (8/50W) with a color temperature of 4000K are used as a light source. The transmission is averaged over an area of approximate  $100 \times 100$  pixels, equivalent to  $0.14 \text{ mm}^2$ . The transmission is averaged over an hour for each pressure, during which the camera has an acquisition frequency of 0.5 Hz. The additional sample of  $\text{Ta}_{50}\text{Pd}_{50}$ , as mentioned in Section [3.1], is used as reference to correct for fluctuations of the light source, and to correct for the optical response of the Pd capping layer. Since the  $\text{Ta}_{0.5}\text{Pd}_{0.5}$  sensing material is insensitive to hydrogen throughout the whole partial pressure range [3], subtracting the response of this sample from the  $\text{Ta}_{1-x}\text{Ru}_x$  samples results in a correction for the response of the Pd capping layer.

### 3.3. RESPONSE TIME MEASUREMENTS

The response times of the samples are measured using the same setup as for the hydrogenography measurements. The samples are exposed to  $1.5 \cdot 10^1 \leq P_{\text{H}_2} \leq 1.0 \cdot 10^4$  from a base pressure of 91 Pa. The samples are kept at each pressure for 2 minutes. The response time of the samples is characterized by the time needed to reach 90% of the final optical transmission.

Gas mixtures	Pressure range (Pa)	Partial H <sub>2</sub> pressure range (Pa)
100% H <sub>2</sub>	$3.3 \cdot 10^3 - 1 \cdot 10^6$	$3.3 \cdot 10^3 - 1 \cdot 10^6$
4% H <sub>2</sub> , 96% Ar	$3.3 \cdot 10^3 - 1 \cdot 10^6$	$1.3 \cdot 10^2 - 4 \cdot 10^4$
0.1% H <sub>2</sub> , 99.9% Ar	$3.3 \cdot 10^3 - 1 \cdot 10^6$	$3.3 - 1 \cdot 10^3$
0.1% H <sub>2</sub> , 99.9% Ar	$9.0 \cdot 10^1 - 9.5 \cdot 10^4$ (l)	$0.1 - 9.5 \cdot 10^1$

Table 3.1: The gas mixtures and pressure ranges used to achieve a total partial hydrogen pressure range of  $1.0 \cdot 10^{-1}$  to  $1.0 \cdot 10^6$  Pa. The rightmost column represents the partial H<sub>2</sub> pressure reached by the pressures in the gas cell (middle column). Settings of the MKS 250 were changed for optimal operation in the lowest pressure range, represented by (l).

### 3.4. EX SITU XRD MEASUREMENTS

The effect of the Ru doping on the structure of Ta<sub>1-x</sub>Ru<sub>x</sub> is studied using ex situ X-Ray Diffraction (XRD) measurements. The apparatus used is a Bruker D8 Discover equipped with a Cu tube and a wavelength of 1.5418Å, with a LynXE detector in 1D mode and a footprint of 0.6 mm. The measurements are performed with a parallel beam geometry, a Gobel mirror, a 0.2 mm exit slit of the source and two 0.2 mm slits on the detector.

We expect the material to be structured in the  $\langle 110 \rangle$  direction with the (1, 1, 0) lattice vector perpendicular to the sample surface, since this is the preferred growth orientation of Ta on a Ti adhesion layer [17]. The measurements are fitted with Pseudo-Voigt functions using the `lmfit` package [18] in Python 3.6.

#### 3.4.1. BRAGG-BRENTANO DIFFRACTOGRAMS

To study the effect of doping on the material using XRD measurements, we use the Bragg-Brentano geometry. As illustrated in Figure [3.2], by using this geometry, the angle between the sample and the incident wave is always equal to the angle between the sample and the scattered wave. This is achieved by moving both arms of the apparatus at the same velocity (counter)clockwise, such that  $\omega = \theta$ . This results in a difference between the wavevectors of the incident and scattered wave  $\mathbf{k} - \mathbf{k}' = \mathbf{G}$  that is equal to an upright reciprocal lattice vector perpendicular to the sample [12]. While the direction of this vector is fixed, its magnitude changes with  $2\theta$ . This allows the observation of diffraction peaks of the coinciding lattice vectors, perpendicular to the sample surface and with the same magnitude.

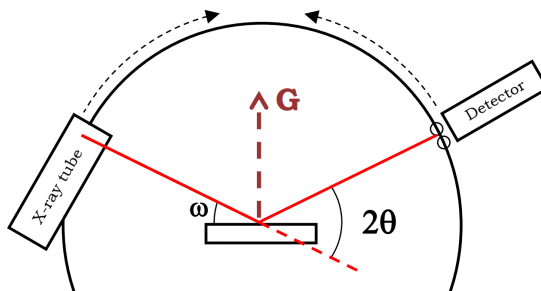


Figure 3.2: Visualisation of the Bragg-Brentano geometry, image from [19]. By moving the X-ray tube and detector (counter)clockwise, the magnitude of the vector  $\mathbf{S}$  varies, allowing the formation of diffraction peaks.

For a thin film of pure Ta, we expect the  $\langle 110 \rangle$  peak at  $2\theta \approx 38$  degrees [17]. To discover if the RuTa, RuTa', RuTa'' phases are present for thin films, we perform the diffraction experiments with  $2\theta$  ranging from 30 to 70 degrees. Using these measurements we can also study the effect of Ru doping on the size of the unit cell and if a solid solution is formed..

### 3.4.2. ROCKING CURVES

In the process of sputtering the samples, it is possible that a nonuniform growth of the crystal structure on the quartz substrate is present. This results in a spread of different crystal plane orientations which is called mosaicity. Using Rocking Curve (RC) measurements we observe the mosaicity of the material or misorientation of atomic planes as broadening of the Rocking Curve [20].

As illustrated in Figure [3.3], RC measurements are performed by keeping the angle  $2\theta$  constant, where  $\omega$  is the angle at which the XRD peak occurs using the Bragg-Brentano geometry. By rocking the arms of the apparatus symmetrically about the vector perpendicular to the sample surface by varying  $0 < \omega < 2\theta$ , the intensity of diffraction due to mosaicity can be observed.

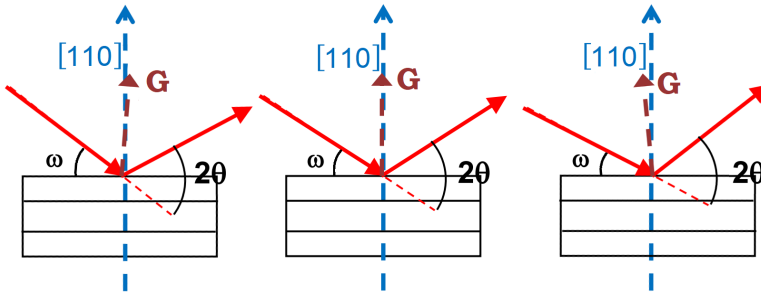


Figure 3.3: Rocking curves measurement illustrated, image from [20]. The vector  $\mathbf{S}$  is rocking symmetrically about the  $\langle 110 \rangle$  vector.

### 3.5. IN SITU XRD MEASUREMENTS

To study the effect of hydrogenation on the structure of both the sensing material and the capping layer, we perform in situ XRD measurements. An Anton Paar XRK 900 reactor chamber is used in combination with the same setup as for ex situ XRD measurements, with the LynXE detector in 0D mode. Bragg-Brentano measurements are performed while the sample is exposed to a hydrogen atmosphere. The partial pressure is varied between  $4.4 \cdot 10^0 \leq P_{H_2} \leq 2.5 \cdot 10^4$  Pa, using a gas mixture of 4%  $H_2$ . The measurements are fitted with Pseudo-Voigt functions using the `lmfit` package in Python 3.6.

### 3.6. IN SITU XRR MEASUREMENTS

In situ X-Ray Reflectometry (XRR) measurements are done along with the in situ XRD measurements. The XRR measurements allow us to determine the thickness of the TaRu and Pd layer. The geometry used in XRR measurements is the same as for the Bragg-

Brentano geometry, but the angle  $2\theta$  is smaller, with  $1 < \theta < 4$  degrees. The reflected waves from different layer interfaces can interfere with each other, which results in the formation of fringes in the reflected signal that are called Kiessing fringes. The thickness of each layer can be determined from the distance between the minima/maxima of this pattern. The XRR data is fitted with GenX3 [21] to find the thickness of each layer.

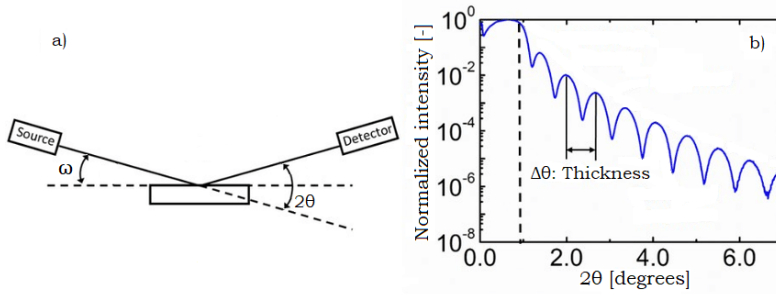


Figure 3.4: Image from [22]. a) Illustration of a XRR measurement, the angle  $2\theta$  is kept constant, with  $1 < \theta < 4$  degrees. b) A typical reflectivity profile. From this profile several material properties can be learned. We are interested in the thickness of each layer, which can be derived using  $\Delta\theta$  between maxima.



# 4

## RESULTS

This Section is dedicated to the results acquired using the experimental methods described in Section [3]. The effect of Ru doping on the optical response and structural properties of  $\text{Ta}_{1-x}\text{Ru}_x$  thin films is studied, as well as the change in structure of the thin films upon/after hydrogenation.

### 4.1. OPTICAL RESPONSE OF THE SENSING MATERIAL

Using hydrogenography measurements, the change in optical transmission upon hydrogenation is studied. The  $\text{Ta}_{1-x}\text{Ru}_x$  sensing layer and Pd capping layer both have an optical response upon hydrogenation. To study the optical response of the  $\text{Ta}_{1-x}\text{Ru}_x$  sensing layer separately, a correction needs to be performed for the Pd capping layer. This correction is done using the additional sample described in Section [3.2]. In Figure [4.1] the effect of correction using the  $\text{Ta}_{0.5}\text{Pd}_{0.5}+\text{Pd}$  thin film is demonstrated. The hydrogenation of the  $\text{Ta}_{1-x}\text{Ru}_x$  sensing layer results in a decrease of optical transmission, while the hydrogenation of the Pd capping layer increases the optical transmission. Subtracting the response of the  $\text{Ta}_{0.5}\text{Pd}_{0.5}+\text{Pd}$  sample from the response of the  $\text{Ta}_{0.9}\text{Ru}_{0.1}+\text{Pd}$  sample results in only the optical response of the  $\text{Ta}_{0.9}\text{Ru}_{0.1}$  sensing layer.

Changes in partial  $\text{H}_2$  pressures are well translated into changes in the optical transmission of the thin film. In Figure [4.2] the change in optical transmission for all  $\text{Ta}_{1-x}\text{Ru}_x$  samples throughout the whole  $10^{-1} - 10^6$  Pa partial pressure range are visualized. A substantial hysteresis is present in the pressure range of  $4 \cdot 10^1 - 4 \cdot 10^4$  Pa (Figure [4.2c]), which will be studied in more detail later. See Appendix (Figure [6.1 - 6.3]) for measurements of the optical response of the samples at all temperatures.

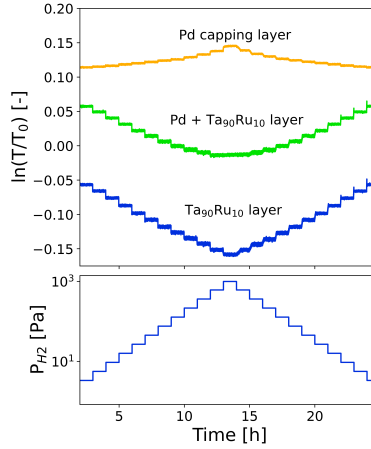


Figure 4.1: Optical response (green) of a 40 nm Ta<sub>0.9</sub>Ru<sub>0.1</sub> sensing layer with a 5 nm Ti adhesion layer on a quartz substrate and a 10 nm Pd capping layer, and (orange) the response of a 40 nm Ta<sub>0.5</sub>Pd<sub>0.5</sub> film with the same adhesion layer, substrate and capping layer. The Ta<sub>0.5</sub>Pd<sub>0.5</sub> sensing layer is insensitive throughout the whole measured pressure range [3], thus the Ta<sub>0.5</sub>Pd<sub>0.5</sub>+Pd optical response is entirely due to the Pd capping layer. Subtracting the response of the Ta<sub>0.9</sub>Ru<sub>0.1</sub>+Pd thin film by the response of the Ta<sub>50</sub>Pd<sub>50</sub>+Pd film results in only the transmission of the Ta<sub>0.9</sub>Ru<sub>0.1</sub> sensing layer. The transmission is plotted relative to the ex situ transmission  $T_0$  and for  $P_{H_2}$  between 10<sup>0</sup> – 10<sup>3</sup> Pa at  $T=28^\circ\text{C}$ .

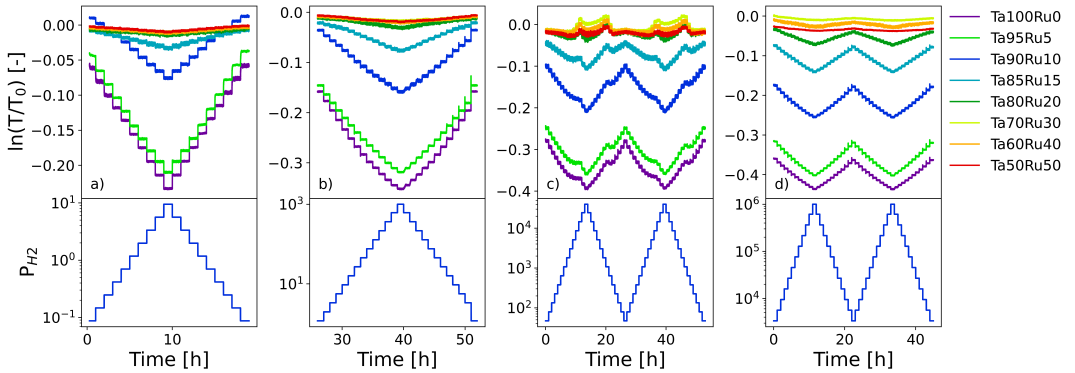


Figure 4.2: Change in optical transmission for the 40 nm Ta<sub>1-x</sub>Ru<sub>x</sub> thin films, with a 5 nm Ti adhesion layer on a quartz substrate and a 10 nm Pd capping layer. The optical response is corrected using the Ta<sub>0.5</sub>Pd<sub>0.5</sub> sample as illustrated in Figure [4.1]. The transmission is relative to the ex situ transmission  $T_0$  and the measurements are performed for partial H<sub>2</sub> pressure ranges of a) 10<sup>-1</sup> – 10<sup>1</sup> Pa, b) 10<sup>0</sup> – 10<sup>3</sup> Pa, c) 4·10<sup>1</sup> – 4·10<sup>4</sup> Pa, d) 10<sup>3</sup> – 10<sup>6</sup> Pa at  $T=28^\circ\text{C}$ .

Combining the change in optical transmission with partial pressure results in a Pressure Transmission Isotherm (PTI). The PTIs for the Ta<sub>1-x</sub>Ru<sub>x</sub> thin films at room temperature are illustrated in Figure [4.3]. As the dopant concentration of Ru is increased, the optical contrast (the difference in transmission between  $P_{H_2}$  minimal and maximal) is decreased. The sensitivity of the sensing layer, which is the slope of the PTI, decreases as the dopant concentration in Ta<sub>1-x</sub>Ru<sub>x</sub> increases (Figure [6.4] in Appendix) for  $P_{H_2}=10^3 - 10^6$ . Notable is the hysteresis at  $P_{H_2} \approx 10^3$  Pa, which occurs for all compositions

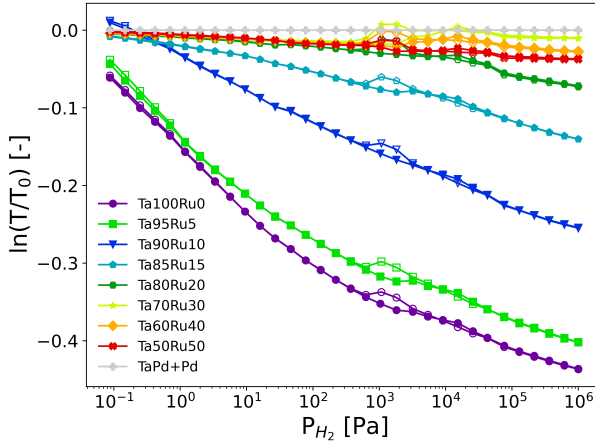


Figure 4.3: Pressure-Transmission Isotherm (PTI) curves for the  $\text{Ta}_{1-x}\text{Ru}_x$  thin films at  $T=28^\circ\text{C}$ . The samples consist of a 40 nm  $\text{Ta}_{1-x}\text{Ru}_x$  sensing layer, a 5 nm Ti adhesion layer on a quartz substrate and a 10 nm Pd capping layer. Each data point is obtained by averaging the optical transmission over 1h at a single pressure, in a partial  $\text{H}_2$  pressure range of  $10^{-1} - 10^6$  Pa. The closed and open data points correspond to increasing and decreasing pressure steps respectively. The optical transmission is relative to ex situ at  $T=28^\circ\text{C}$ .

with the same shape. Since the  $\text{Ta}_{0.9}\text{Ru}_{0.1}$  thin film has the most linear response throughout the pressure range and a significant decrease of  $\sim 25\%$  in optical transmission, this composition is studied in more detail.

The optical contrast of  $\text{Ta}_{0.9}\text{Ru}_{0.1}$  is similar to  $\text{Ta}_{1-x}\text{Pd}_x$  [3]. Changing the Ru dopant concentration changes the optical contrast of  $\text{Ta}_{1-x}\text{Ru}_x$  for the measured pressure range, in contrast to  $\text{Ta}_{1-x}\text{Pd}_x$ . In Figure [4.4] the optical contrast is plotted as a function of dopant concentration at  $P_{\text{H}_2} = 4.3 \cdot 10^4$  Pa. We see that the contrast decreases linearly with increasing  $x$  in  $\text{Ta}_{1-x}\text{Ru}_x$  until  $x=0.2$ . Assuming a linear relationship between the partial pressure to which the thin films are exposed and their hydrogen content (observed for Ta at  $10^{-1} \leq P_{\text{H}_2} \leq 10^2$  Pa [5]), doping Ta with Ru thus linearly influences the hydrogenation of the sensing layer for  $x \leq 0.2$ .

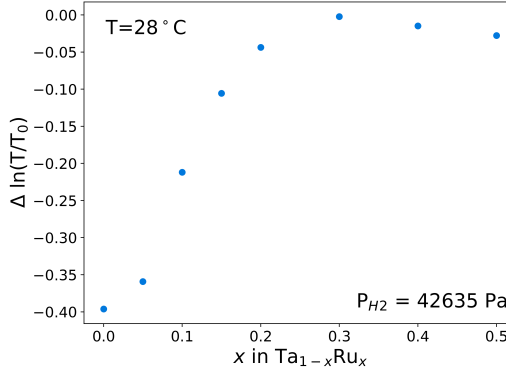


Figure 4.4: Optical contrast of the  $\text{Ta}_{1-x}\text{Ru}_x$  thin films at a partial pressure of  $P_{H_2}=42635$  Pa. The samples consist of a 40 nm  $\text{Ta}_{1-x}\text{Ru}_x$  sensing layer, a 5 nm Ti adhesion layer on a quartz substrate and a 10 nm Pd capping layer. Each data point is obtained by averaging the optical transmission over 1h. The contrast is relative to the optical transmission ex situ at  $T=28^\circ\text{C}$ .

To study the effect of temperature on the optical response of the samples and how the  $\text{Ta}_{1-x}\text{Ru}_x$  thin films operate for higher partial pressures, PTIs are made at temperatures  $T=28 - 120^\circ\text{C}$ . As displayed in Figure [4.5a], the optical contrast of the  $\text{Ta}_{0.9}\text{Ru}_{0.1}$  sensing layer practically remains constant. The optical contrast of the  $\text{Ta}_{1-x}\text{Ru}_x$  thin films for  $0.05 \leq x \leq 0.2$  also does not change for increasing temperatures (Figure [6.5] in Appendix). An increase of temperature results in the shift of the PTI to higher partial pressures, while  $\ln(T/T_0)$  still changes linearly with  $P_{H_2}$ . Comparing the optical contrast of  $\text{Ta}_{0.9}\text{Ru}_{0.1}$  with Ta (Figure [4.5b]), we see that the contrast of the Ta thin film is larger, and that it increases with for elevated temperatures, confirming the results of Ref.[5]. Positive values for  $\ln(T/T_0)$  are due to incorrect normalization of the optical transmission.

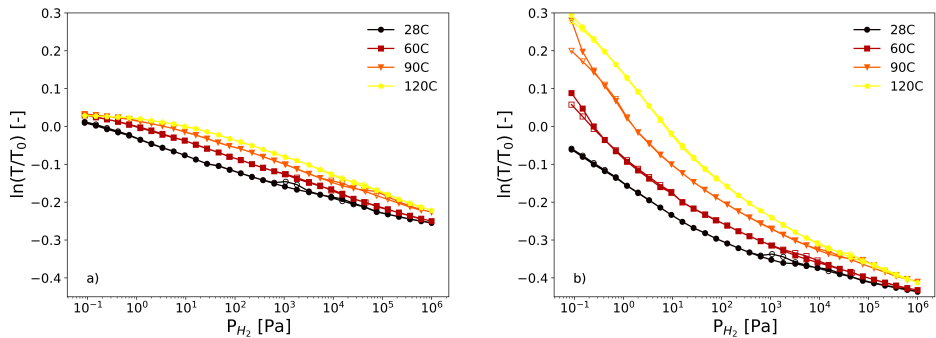


Figure 4.5: PTI curves at  $T=28 - 120^\circ\text{C}$  for 40 nm a)  $\text{Ta}_{0.9}\text{Ru}_{0.1}$  and b) Ta thin films on a quartz substrate with a 5 nm Ti adhesion layer and a 10 nm Pd capping layer. Each data point is obtained by averaging the optical transmission over 1h at a single pressure, in a partial  $\text{H}_2$  pressure range of  $10^{-1} - 10^6$  Pa. The optical transmission is relative to ex situ at  $T=28^\circ\text{C}$ . The open and closed data points respectively represent increasing and decreasing pressure steps.

The response of the  $\text{Ta}_{0.9}\text{Ru}_{0.1}$  thin film is displayed in Figure [4.6a] for pressure steps to  $1 \cdot 10^2 - 2 \cdot 10^3$  Pa. The normalisation of the response is defined with the final transmission being equal to 1. The overshoot of the response grows as the pressure step becomes bigger. This is because the hydrogenation of the Pd capping layer leads to a perturbation of the optical response, which increases for larger pressures steps. Since the Pd capping layer also has an optical response due to hydrogenation which is slower than the  $\text{Ta}_{0.9}\text{Ru}_{0.1}$  sensing layer, the measurements for  $P_{H_2} > 2 \cdot 10^3$  Pa are not interpretable for the response time of  $\text{Ta}_{0.9}\text{Ru}_{0.1}$ .

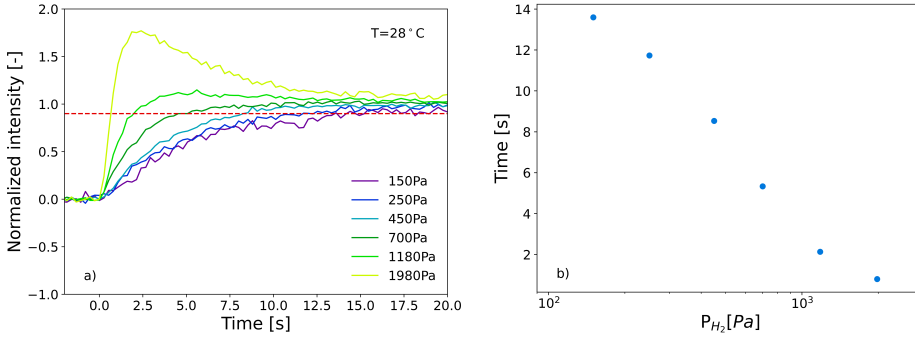


Figure 4.6: Measurements at  $T=28^\circ\text{C}$  of a) the optical response of the  $\text{Ta}_{0.9}\text{Ru}_{0.1}$  sample upon increasing pressure steps. The response time is characterized by the time needed to reach 90% of the final transmission, as indicated by the red line. b) The response time of the  $\text{Ta}_{0.9}\text{Ru}_{0.1}$  sample plotted for  $P_{H_2}=1 \cdot 10^2 - 2 \cdot 10^3$  Pa.

The response time is characterized by the time that is needed to reach 90% of the final transmission due to the pressure increase, which is indicated by the red dashed line. The pressure dependency of the response time is illustrated in Figure [4.6b]. A decrease in response time is observed when the pressure step size increases, which is also observed for Pd capped Ta thin films [23].

## 4.2. STRUCTURAL MEASUREMENTS

The effect of Ru doping on the structure of the sensing material before hydrogenation is illustrated in Figure [4.7a]. The  $\langle 110 \rangle$   $\text{Ta}_{1-x}\text{Ru}_x$  peaks from the sensing layer can be seen and  $\langle 111 \rangle$  Pd peak from the capping layer [23]. As no other diffraction peaks are observed, no additional phases are present. As the  $\text{RuTa}$ ,  $\text{RuTa}'$ ,  $\text{RuTa}''$  phases are not formed, the phase diagram for thin film  $\text{Ta}_{1-x}\text{Ru}_x$  is different from bulk.

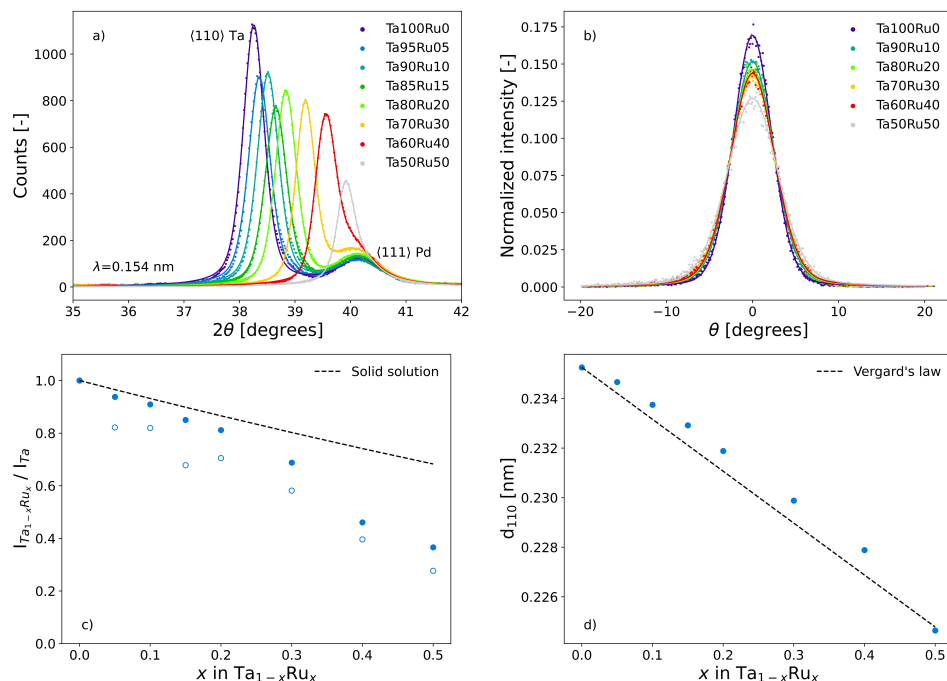


Figure 4.7: Results of ex situ XRD measurements at  $T=28^\circ\text{C}$  in air of 40 nm  $\text{Ta}_{1-x}\text{Ru}_x$  thin films with a 5 nm Ti adhesion layer on a quartz substrate and a 10 nm Pd capping layer (Cu anode,  $\lambda=0.154$  nm). The measurements are performed before they are exposed to hydrogen cycles. a) Bragg-Brentano diffractograms of the samples with fits of the data using two pseudo-Voigt functions. b) Rocking Curve measurements of the  $\langle 110 \rangle$   $\text{Ta}_{1-x}\text{Ru}_x$  peak with a fit of the data using a single pseudo-Voigt function. c) Dependence of the intensity of the  $\text{Ta}_{1-x}\text{Ru}_x$   $\langle 110 \rangle$  peak on the dopant concentration in  $\text{Ta}_{1-x}\text{Ru}_x$ . The intensity of each peak is relative to the intensity of the Ta peak. The intensities are corrected for the broadening i.e. the increase of the FWHM of the Rocking Curve for each  $\text{Ta}_{1-x}\text{Ru}_x$  sample, and are relative to the intensity of the Ta peak. The open and closed data points represent the relative intensity before and after the correction respectively. The decrease of the diffraction peak intensity according to a solid solution is indicated by the dashed line. d) Dependence of the  $d_{110}$  spacing on  $x$  in  $\text{Ta}_{1-x}\text{Ru}_x$ . The relation between the dopant concentration and the  $d_{110}$  spacing is plotted with the dashed line using Vegard's law.

With increasing dopant concentration, the  $\langle 110 \rangle$  Ta peak shifts to higher diffraction angles, indicating a decrease of the  $d_{110}$  spacing. This decrease is expected, as Ru has a lower atomic radius than Ta. To incorporate the Ru atom with a different atomic radius in the metal, the crystal lattice contracts.

In Figure [4.7d] the decrease of the unit cell size with dopant concentration is plotted, together with Vegard's law. As endpoints for Vegard's law the  $d_{110}$  spacing of Ta and the calculated  $d_{110}$  spacing of Ru used. The Ru spacing is obtained using a separate measurement of sputtered Ru on a Ti adhesion layer from Ref.[23]. The decrease of the unit cell size approximately follows Vegard's law.

In Figure [4.7b] the Rocking Curves are plotted, in which the broadening of these curves can be seen. This indicates that the mosaicity increases with dopant concentration.

The intensity of the  $\langle 110 \rangle$   $\text{Ta}_{1-x}\text{Ru}_x$  peak relative to the Ta peak is plotted in Figure [4.7c] as a function of dopant concentration. The intensity is corrected for the loss of intensity due to the broadening of the Rocking Curves. The expected change in diffraction peak intensity with dopant concentration for a solid solution is calculated using Eq.[2.7] in Section [2.5]. For  $x \leq 0.2$  in  $\text{Ta}_{1-x}\text{Ru}_x$  the decrease in intensity is approximately according a solid solution, suggesting the formation of a solid solution.

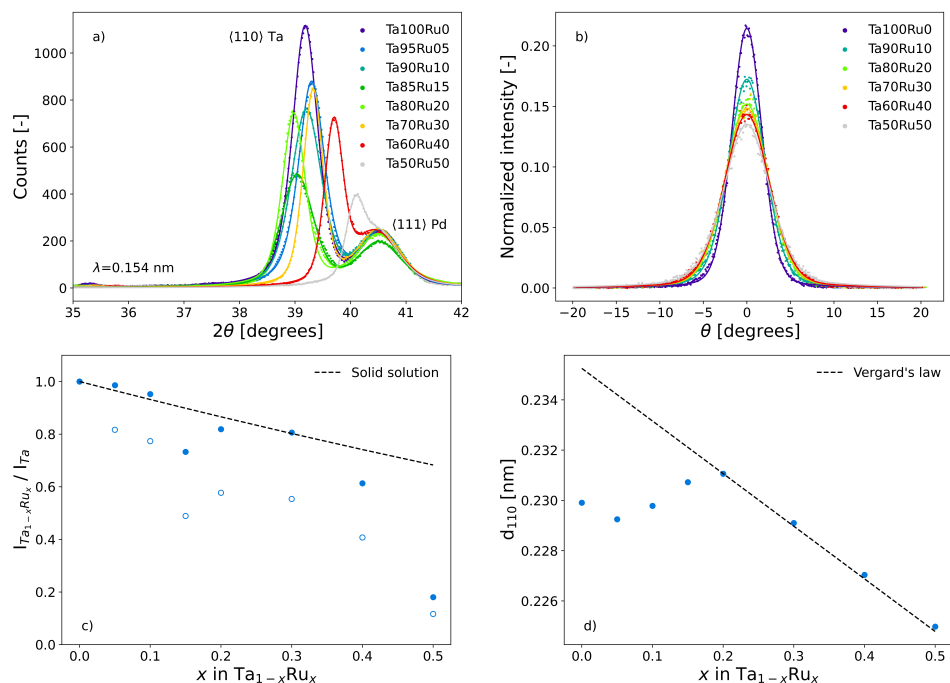


Figure 4.8: Ex situ XRD measurements at  $T=28^\circ\text{C}$  in air after hydrogenation cycles of 40 nm Ta<sub>1-x</sub>Ru<sub>x</sub> thin films with a 5 nm Ti adhesion layer on a quartz substrate and a 10 nm Pd capping layer. A Cu anode is used with  $\lambda=0.154$  nm. a) Results of Bragg-Brentano measurements of the samples, fitted with two pseudo-Voigt functions. b) Rocking Curves of the  $\langle 110 \rangle$  Ta<sub>1-x</sub>Ru<sub>x</sub> peak, with each curve normalized by the intensity of each peak. The data is fitted with a single pseudo-Voigt function. c) Dependence of the intensity of the Ta<sub>1-x</sub>Ru<sub>x</sub>  $\langle 110 \rangle$  peak on the dopant concentration in Ta<sub>1-x</sub>Ru<sub>x</sub>. The intensity of each peak is relative to the intensity of the Ta peak. The intensities are corrected for the broadening, a increase of the FWHM, of the Rocking Curve for each Ta<sub>1-x</sub>Ru<sub>x</sub> sample, relative to Ta. The open and closed data points represent the relative intensity before and after the correction respectively. The decrease of the diffraction peak intensity according to a solid solution is indicated by the dashed line. d) Dependence of the  $d_{110}$  spacing on the doping in Ta<sub>1-x</sub>Ru<sub>x</sub>. The relation between the dopant concentration and the  $d_{110}$  spacing is plotted with the dashed line using Vegard's law.

XRD measurements are again done after exposing the Ta<sub>1-x</sub>Ru<sub>x</sub> thin films to hydrogenation cycles, which are displayed in Figure [4.8a]. These cycles allow the microstructure of the material to settle, allowing for some structural changes. As can be seen in Figure [4.8d], the resettling mostly affects the compositions with  $x \leq 0.15$  in Ta<sub>1-x</sub>Ru<sub>x</sub>, with the result that Vegard's law falls apart in this region of dopant concentration. The decrease in intensity of the Ta<sub>1-x</sub>Ru<sub>x</sub> diffraction peak is shown in Figure [4.8c], together with the same relations stated earlier. A correction is applied depending on the broadening of the Rocking Curve (Figure [4.8b]). The decrease of intensity appears to be according to a solid solution, implying that a solid solution is formed. Measurements of Ta<sub>1-x</sub>Ru<sub>x</sub> with more compositions for  $0 \leq x \leq 0.3$  are needed to support this statement.

The in situ XRD measurements in Figure [4.9a] indicate that upon hydrogenation, the

$\text{Ta}_{1-x}\text{Ru}_x$  diffraction peak shifts linearly to lower diffraction angles, indicating a steady increase of the unit cell size. The  $(111)$  Pd peak also shifts to lower angles but disappears. A new Pd phase is formed; the  $\alpha'$ -Pd phase [24] (also called the  $\beta$ -Pd phase). Figure [4.9b] shows the expansion of the unit cell relative to in air, with an increase of 6.4% for  $P_{\text{H}_2} = 2.5 \cdot 10^4$ . A difference in expansion between loading and unloading pressure steps is visible. Hysteresis in the expansion of the unit cell typically is due to the extra energy needed to accommodate hydrogen in the sensing material. No hysteresis is thus present, as the expansion of the unit cell is larger for loading pressure steps than for unloading pressure steps. The difference in expansion could be due to measurement error.

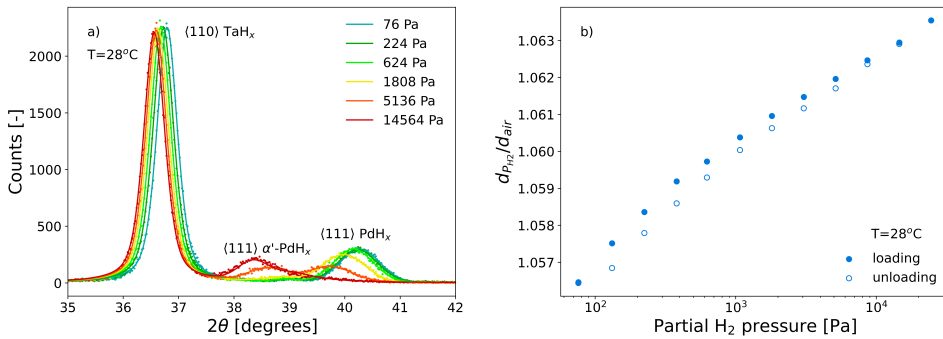


Figure 4.9: In situ XRD measurements of a 40nm Ta thin film with a 5 nm Ti adhesion layer on a quartz substrate and a 10 nm Pd capping layer at  $T=28^\circ\text{C}$ . a) Bragg-Brentano diffractograms with a Cu anode of  $\lambda = 0.154$  nm for increasing pressure steps. The data is fitted with three pseudo-Voigt functions. b) The dependence of the  $d_{110}$  spacing on the partial  $\text{H}_2$  pressure. The spacing is relative to the spacing of the  $\text{Ta}_{100}\text{Ru}_0$  sample as measured in air at  $T=28^\circ\text{C}$ .

To study the effect of doping on the hydrogenation of the sensing material, in situ XRD measurements at  $T=28^\circ\text{C}$  and  $P_{\text{H}_2}=5.3 \cdot 10^3$  Pa are made (Figure [4.10a]). The expansion of the unit cell upon hydrogenation is linearly dependent on dopant concentration for  $x \leq 0.15$  in  $\text{Ta}_{1-x}\text{Ru}_x$  (Figure [4.10b]). The amplitude of the diffraction peaks however have a nonlinear decrease. The  $\alpha'$ -Pd $\text{H}_x$  phase is present for  $x < 0.5$  in  $\text{Ta}_{1-x}\text{Ru}_x$  but unexpectedly is suppressed completely for  $x=0.5$ .

The unit cell size decrease explains the decrease in optical contrast for the same range of  $x$  (Figure [4.4]). As the unit cell size decreases, the solubility of hydrogen decreases in the sensing material for the measured pressure range, affecting the maximal change in optical transmission. This effect of alloying on the optical contrast is also observed with the alloying of Pd [2].

XRR measurements are performed to determine the expansion of the thin film upon hydrogenation, which are displayed in Figure [4.11a]. The  $\text{Ta}_{1-x}\text{Ru}_x$  sensing layer expands 8.6% for  $P_{\text{H}_2} = 2.5 \cdot 10^4$ . The  $d_{110}$  spacing increases 6.4% for the same pressure, which would result in a volumetric expansion of the unit cell of 20% if the expansion is the same in all directions. Since the 20% volumetric expansion of the unit cell is not translated into a 20% increase of the  $\text{Ta}_{1-x}\text{Ru}_x$  sensing layer thickness, the unit cell of

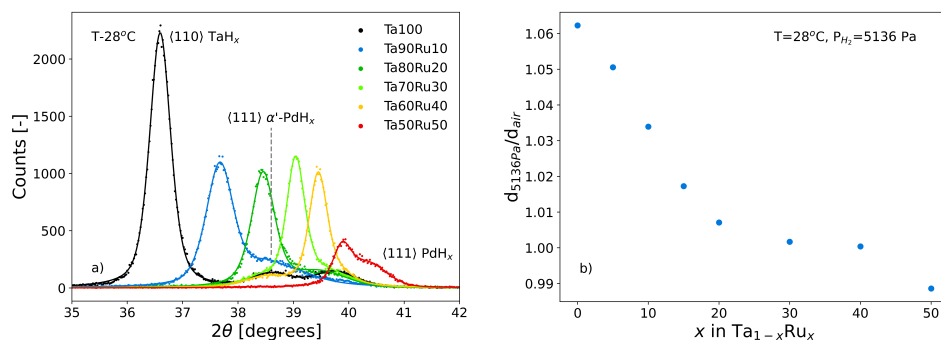


Figure 4.10: In situ XRD measurements of 40 nm  $\text{Ta}_{1-x}\text{Ru}_x$  thin films with a 5 nm Ti adhesion layer on a quartz substrate and a 10 nm Pd capping layer at  $T=28^\circ$  and  $P_{\text{H}_2}=5136$  Pa (Cu anode,  $\lambda=0.154$  nm). a) Diffraction patterns of the  $\text{Ta}_{1-x}\text{Ru}_x$  samples and b) the dependence of the unit cell size on dopant concentration.

$\text{Ta}_{1-x}\text{Ru}_x$  does not expand equally in all directions.

The change of the Pd capping layer thickness is displayed in Figure [4.11b], where we first observe that while the layer does expand with increasing hydrogen content, the layer thickness first is smaller than in air which is unexpected. A noticeable hysteresis is present in the expansion of the capping layer, with a maximal difference of  $\sim 3\%$  between the loading and unloading thickness. This hysteresis is due to the formation of  $\alpha'$ PdH<sub>x</sub>, as we observe a phase transition of Pd in the region  $P_{\text{H}_2} = 10^3 - 10^4$  Pa (Figure [4.9a]).

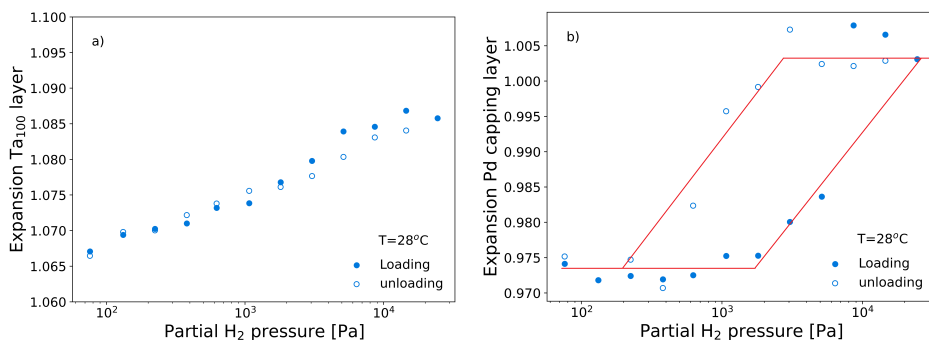


Figure 4.11: Results of XRR measurements from a 40 nm  $\text{Ta}_{100}\text{Ru}_0$  thin film with a 5 nm Ti adhesion layer on a quartz substrate and a 10 nm Pd capping layer at  $T=28^\circ\text{C}$  and  $P_{\text{H}_2}$  between  $8 \cdot 10^1 - 2 \cdot 10^4$  Pa (Cu anode,  $\lambda=0.154$  nm). a) Expansion of the  $\text{Ta}_{100}\text{Ru}_0$  sensing layer with partial  $\text{H}_2$  pressure and b) Expansion of the Pd capping with partial  $\text{H}_2$  pressure. The red line serves as a guide to the eye.

# 5

## DISCUSSION

The effect of Ru doping on the structure of  $Ta_{1-x}Ru_x$  and the effect of nanoconfinement on  $Ta_{1-x}Ru_x$  is studied. As indicated in Section [4.2], ex situ XRD measurements reveal no additional phases in the sensing layer when measured before (Figure [4.7]) and after (Figure [4.8]) exposure to hydrogen, which confirms that a thin film is formed in a single crystalline phase. This indicates that the RuTa, RuTa', RuTa'' phases are not present due to nanoconfinement.

The large decrease in diffraction peak intensity may suggest the presence of additional amorphous phases. A decrease of the unit cell size is observed upon increasing dopant concentration. After hydrogenation, this decrease does not follow Vegard's law for  $x < 0.2$  in  $Ta_{1-x}Ru_x$ . The ex situ XRD measurements after hydrogenation imply that a solid solution is formed.

While the in situ XRD measurements do not reveal any phase transition of the  $Ta_{1-x}Ru_x$  sensing layer, there is a phase transition of Pd to  $\alpha'$ -Pd in the capping layer upon hydrogenation. The phase transition results in hysteresis in the expansion of the Pd capping layer. This leads to the dependency of hydrogen absorption on pressure history, resulting in hysteresis in the hydrogenation of the sensing material.

Increasing the Ru dopant concentration results in a decrease in the amount of hydrogen that is absorbed in the sensing material.

To use  $Ta_{1-x}Ru_x$  as a material for hydrogen sensing, it needs to meet certain requirements, as stated in Section [2.1]. First off all, we want our sensing material to have a large sensing range. The PTIs of  $Ta_{1-x}Ru_x$  at  $T=28^\circ\text{C}$  show a gradual change in optical transmission over 7 orders of partial  $P_{H_2}$  pressure range for  $x \leq 0.1$  in  $Ta_{1-x}Ru_x$ .

As predicted by the law of Lambert-Beer (Section [2.3]), the PTI of  $Ta_{1-x}Ru_x$  at room temperature shows a linear relationship between  $\ln(T/T_0)$  and  $P_{H_2}$ . This linear relationship holds at elevated temperatures, and the PTI is shifted to higher pressures for an increase of temperature. The optical contrast of  $Ta_{0.9}Ru_{0.1}$  is also quite large, with an decrease of 25% in optical transmission upon hydrogenation.

The PTIs of  $Ta_{1-x}Ru_x$  at elevated temperatures show that the optical contrast does not change with an increase in temperature. As the measurements at higher temperatures translate to higher pressures and the optical contrast remains constant, doping Ta with Ru results in a hydrogenation of the sensing layer at higher pressures. Increasing the Ru dopant concentration in  $Ta_{1-x}Ru_x$  thus results in a shift of the sensing range to higher partial pressures, so changing this concentration can be used to tune the pressure range of  $Ta_{1-x}Ru_x$ .

For an effective hydrogen sensor we additionally do not want any dependency of the thin films on the pressure history. In the PTIs of the  $Ta_{1-x}Ru_x$  thin films we however discover hysteresis in the region of  $P_{H_2} \simeq 10^3$  Pa for all compositions.

This dependency could be due to the  $Ta_{1-x}Ru_x$  layer not being formed in a single phase, or due to phase transitions of the sensing or Pd capping layer upon hydrogenation. An additional cause could be the large stresses generated by clamping of the  $Ta_{1-x}Ru_x$  layer to the substrate due to large expansion of the thin film upon hydrogenation [25].

As the phase transition of the Pd capping layer is in the same pressure range as the hysteresis in the optical response, this phase transition is the cause of this pressure dependency. Alloying the Pd capping layer with Cu and Au results in a complete suppression of the Pd phase transition [3], which would lead to a hysteresis-less optical response of the sensor.

The optical response of the  $Ta_{0.9}Ru_{0.1}$  sensing layer is quite fast with response times of maximal 15 seconds for  $P_{H_2} = 1.5 \cdot 10^2 - 2.0 \cdot 10^3$  Pa, a significant improvement from pure Ta thin films [5]. The response time of the sensor quickly decreases as the pressure to which the sensor is exposed increases, which is also observed for Pd capped Ta. If the optical response of the capping layer is not taken into account, these measurements suggest a sub-second response time for  $P_{H_2} \geq 2.0 \cdot 10^3$ . As performed in Ref.[3], alloying the Pd capping layer with Cu and Au results in no optical contrast of this layer upon hydrogenation. Performing response time measurements with this capping layer composition would result in the real response time of the  $Ta_{0.9}Ru_{0.1}$  sensing layer. Adding an additional PTFE layer on top of the Pd capping layer could improve the rate at which hydrogen is absorbed by the capping layer from 4 to 15 times [23], depending on the Ru dopant concentration. This would result in even faster response times than  $Ta_{1-x}Pd_x$ .

With the alloying of the Pd capping layer and additional PTFE coating, we deem  $Ta_{0.9}Ru_{0.1}$  as an effective material for hydrogen sensing, with a sensing range of 7 orders of magnitude in pressure, short response times and no hysteresis.

# 6

## CONCLUSION

From the optical response of  $\text{Ta}_{1-x}\text{Ru}_x$  and the change in structure upon hydrogenation, we conclude that  $\text{Ta}_{0.9}\text{Ru}_{0.1}$  is an effective material for hydrogen sensing. Changes in partial  $\text{H}_2$  pressure are well translated in to a change in optical transmission. The PTI of  $\text{Ta}_{0.9}\text{Ru}_{0.1}$  reveals a gradual change in optical transmission upon hydrogenation over 7 orders of magnitude in  $P_{\text{H}_2}$ .

While a significant hysteresis is observed in the optical response of the Pd capped  $\text{Ta}_{1-x}\text{Ru}_x$  thin films, in situ XRD measurements also reveal a phase transition of the Pd capping layer and a sizeable hysteresis in its expansion for the same pressure range. The pressure dependency of the thin films is thus due to the phase transition of the Pd capping layer upon hydrogenation. Alloying the Pd capping layer would prevent this phase transition, leading to a hysteresis-less optical response.

The nanoconfinement of  $\text{Ta}_{1-x}\text{Ru}_x$  as a thin film leads to a suppression of the transition to other crystalline material phases. We additionally found that the  $\text{Ta}_{1-x}\text{Ru}_x$  thin films form a solid solution for  $0 \leq x \leq 0.3$  in  $\text{Ta}_{1-x}\text{Ru}_x$ .

Comparing the optical response of  $\text{Ta}_{1-x}\text{Ru}_x$  to  $\text{Ta}_{1-x}\text{Pd}_x$ , we observe a similar optical contrast. An increasing in temperature does not change the optical contrast of  $\text{Ta}_{1-x}\text{Ru}_x$ , but shifts the PTI to higher partial pressures. The PTIs of  $\text{Ta}_{1-x}\text{Ru}_x$  for  $0 \leq x \leq 0.2$  show a constant optical contrast with increasing temperatures, implying that the hydrogen solubility is not decreased upon alloying. The hydrogenation of the sensing layer thus happens at higher partial pressures, resulting in a shift of the sensing range to higher pressures. To further study the tuning of the sensing range, PTIs of  $\text{Ta}_{1-x}\text{Ru}_x$  need to be measured for more compositions of  $0 \leq x \leq 0.2$ .

The  $\text{Ta}_{0.9}\text{Ru}_{0.1}$  thin film features a response time under 15 seconds at room temperature which decreases for increasing  $P_{\text{H}_2}$ . Coating the Pd capping layer with a PTFE layer could increase response times significantly, even to a shorter response time than  $\text{Ta}_{1-x}\text{Pd}_x$ .

To examine the lifetime of the sensor, the optical response of the sensor needs to be studied over a large number of hydrogen cycles. To ensure a stable and reproducible sensor response, the optical response of the sensor needs to be identical for all hydrogen cycles. We recommend alloying the Pd capping layer and the use of a PTFE coating to achieve a hysteresis free optical response of  $\text{Ta}_{0.9}\text{Ru}_{0.1}$ , with a sensing range of at least 7 orders of magnitude in pressure and a sub-second response time. These improvements would prove  $\text{Ta}_{0.9}\text{Ru}_{0.1}$  to be an effective material for hydrogen sensing.

# APPENDIX

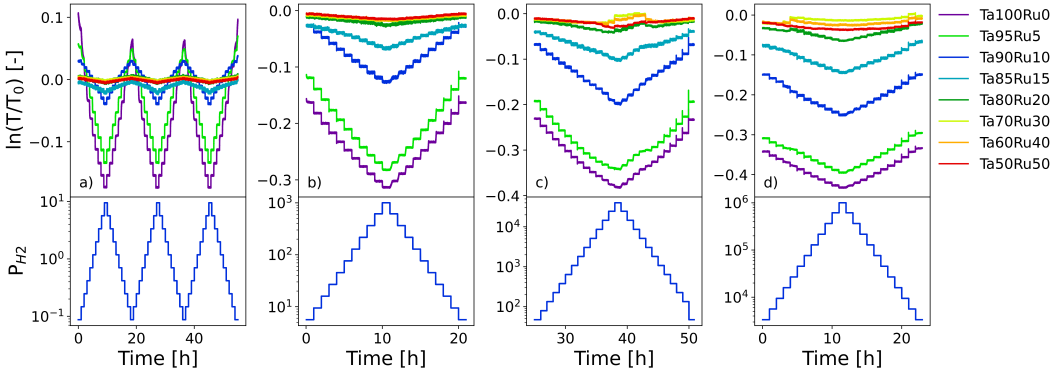


Figure 6.1: Change in optical transmission for the 40 nm  $\text{Ta}_{1-x}\text{Ru}_x$  thin films, with a 5 nm Ti adhesion layer on a quartz substrate and a 10 nm Pd capping layer. The optical response is corrected using the  $\text{Ta}_{0.5}\text{Pd}_{0.5}$  sample as illustrated in Figure [4.1]. The transmission is relative to the ex situ transmission  $T_0$  and the measurements are performed for partial  $\text{H}_2$  pressure ranges of a)  $10^{-1} - 10^1$  Pa, b)  $10^0 - 10^3$  Pa, c)  $4 \cdot 10^1 - 4 \cdot 10^4$  Pa, d)  $10^3 - 10^6$  Pa at  $T=60^\circ\text{C}$ .

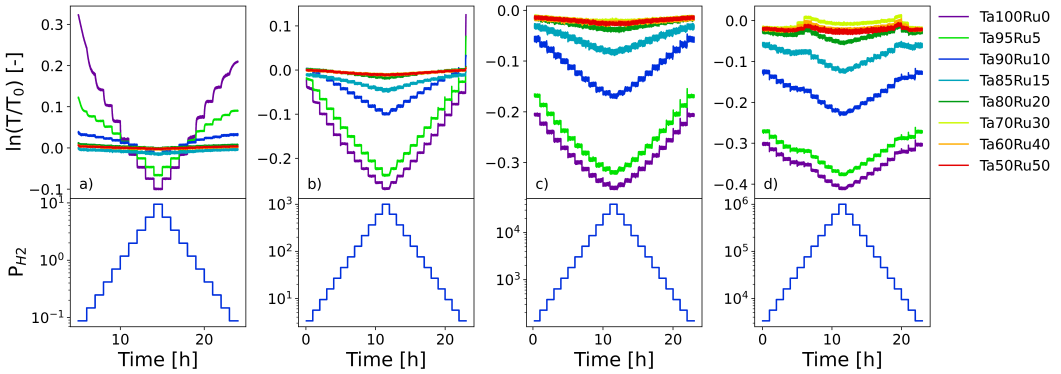


Figure 6.2: Change in optical transmission for the 40 nm  $\text{Ta}_{1-x}\text{Ru}_x$  thin films, with a 5 nm Ti adhesion layer on a quartz substrate and a 10 nm Pd capping layer. The optical response is corrected using the  $\text{Ta}_{0.5}\text{Pd}_{0.5}$  sample as illustrated in Figure [4.1]. The transmission is relative to the ex situ transmission  $T_0$  and the measurements are performed for partial  $\text{H}_2$  pressure ranges of a)  $10^{-1} - 10^1$  Pa, b)  $10^0 - 10^3$  Pa, c)  $4 \cdot 10^1 - 4 \cdot 10^4$  Pa, d)  $10^3 - 10^6$  Pa at  $T=90^\circ\text{C}$ .

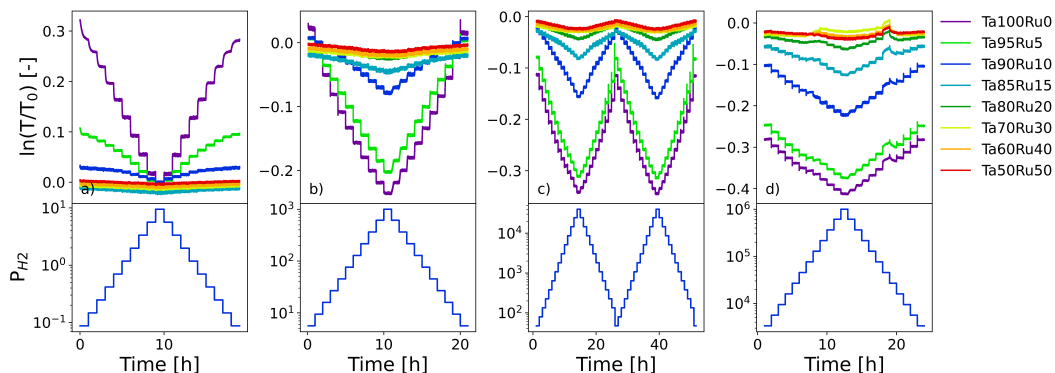


Figure 6.3: Change in optical transmission for the 40 nm  $\text{Ta}_{1-x}\text{Ru}_x$  thin films, with a 5 nm Ti adhesion layer on a quartz substrate and a 10 nm Pd capping layer. The optical response is corrected using the  $\text{Ta}_{0.5}\text{Pd}_{0.5}$  sample as illustrated in Figure [4.1]. The transmission is relative to the ex situ transmission  $T_0$  and the measurements are performed for partial  $\text{H}_2$  pressure ranges of a)  $10^{-1} - 10^1$  Pa, b)  $10^0 - 10^3$  Pa, c)  $4 \cdot 10^1 - 4 \cdot 10^4$  Pa, d)  $10^3 - 10^6$  Pa at  $T=120^\circ\text{C}$ .

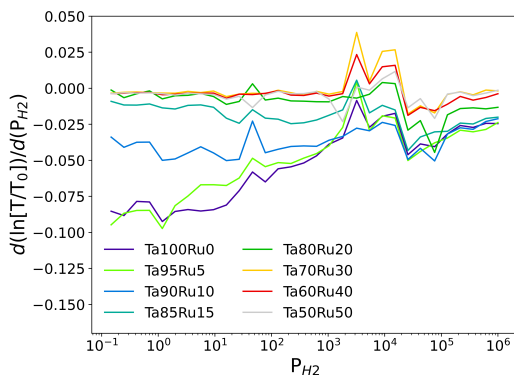


Figure 6.4: Sensitivity of the 40 nm  $\text{Ta}_{1-x}\text{Ru}_x$  thin films, with a 5 nm Ti adhesion layer on a quartz substrate and a 10 nm Pd capping layer. The sensitivity is calculated as the finite difference between the optical transmission and partial  $\text{H}_2$  pressure. The transmission is relative to the ex situ transmission  $T_0$  and the measurements are performed at  $T=28^\circ\text{C}$ .

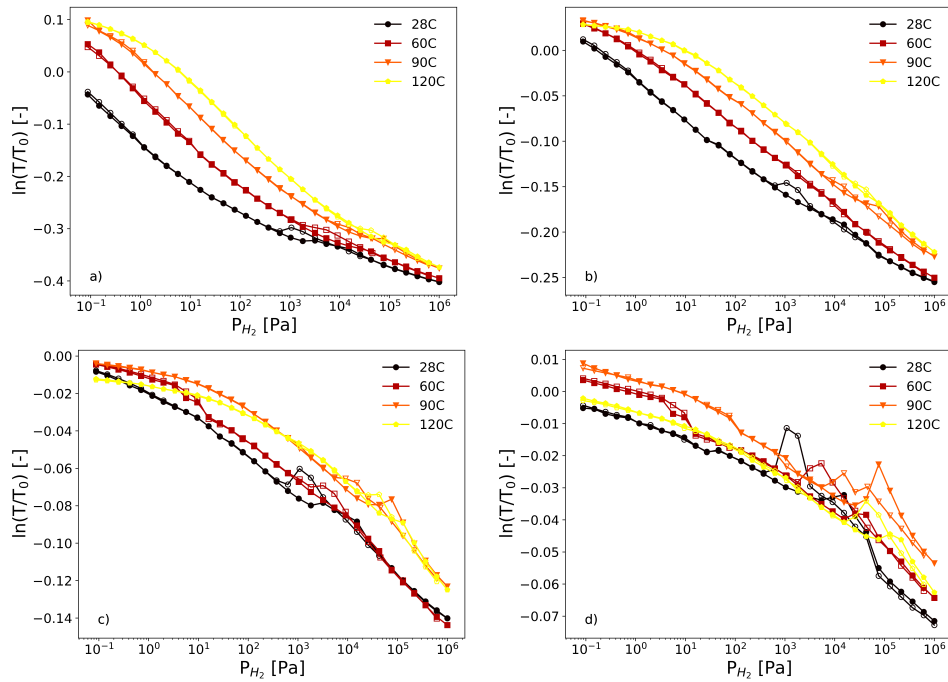


Figure 6.5: PTI curves at  $T=28-120^{\circ}\text{C}$  for 40 nm a)  $\text{Ta}_{0.95}\text{Ru}_{0.05}$ , b)  $\text{Ta}_{0.90}\text{Ru}_{0.1}$ , c)  $\text{Ta}_{0.85}\text{Ru}_{0.15}$ , d)  $\text{Ta}_{0.80}\text{Ru}_{0.20}$  thin films on a quartz substrate with a 5 nm Ti adhesion layer and a 10 nm Pd capping layer. Each data point is obtained by averaging the optical transmission over 1h at a single pressure, in a partial  $\text{H}_2$  pressure range of  $10^{-1} - 10^6$  Pa. The optical transmission is relative to ex situ at  $T=28^{\circ}\text{C}$ . The open and closed data points respectively represent increasing and decreasing pressure steps.



# REFERENCES

- [1] Gasunie, *Gasunie and hydrogen*, Accessed 27-7-21, <https://www.gasunie.nl/en/energy>.
- [2] L.J. Bannenberg et al., *Metal (boro-) hydrides for high energy density storage and relevant emerging technologies*, *International Journal of Hydrogen Energy* **45**, 33687 (2020).
- [3] L. Bannenberg, H. Schreuders, and B. Dam, *Tantalum-palladium: Hysteresis-free optical hydrogen sensor over 7 orders of magnitude in pressure with sub-second response*, *Advanced Functional Materials* **31**, 2010483.
- [4] L. J. Bannenberg, C. Boelsma, K. Asano, H. Schreuders, and B. Dam, *Metal hydride based optical hydrogen sensors*, *Journal of the Physical Society of Japan* **89**, 051003 (2020).
- [5] L. Bannenberg, C. Boelsma, H. Schreuders, S. Francke, N. Steinke, A. van Well, and B. Dam, *Optical hydrogen sensing beyond palladium: Hafnium and tantalum as effective sensing materials*, *Sensors and Actuators B: Chemical* **283**, 538 (2019).
- [6] B. Predel, *Ru-Ta (Ruthenium-Tantalum): Datasheet from Landolt-Börnstein - Group IV Physical Chemistry, Phase Equilibria, Crystallographic and Thermodynamic Data of Binary Alloys* **5J**, 10.1007/10551312\_2639.
- [7] Y. Pivak, *Validation of hydrogenography for the search of promising hydrogen storage materials*, *Ph.D. thesis*, Delft University of Technology (2012).
- [8] N. Taşaltın, S. Öztürk, N. Kılınç, and Z. Z. Öztürk, *Investigation of the hydrogen gas sensing properties of nanoporous Pd alloy films based on AAO templates*, *Journal of Alloys and Compounds* **509**, 4701 (2011).
- [9] B. D. Adams and A. Chen, *The role of palladium in a hydrogen economy*, *Materials Today* **14**, 282 (2011).
- [10] H. Okamoto, *Ru-Ta (Ruthenium-Tantalum)*, *Journal of Phase Equilibria* **12**, 395 (1991).
- [11] K. Jacob, S. Raj, and L. Rannesh, *Vegard's law: A fundamental relation or an approximation?* *International Journal of Materials Research* **98** (2007), 10.3139/146.101545.
- [12] A. Akhmerov, *X-ray diffraction, reciprocal lattice: Laue conditions*, *Open Solid State Notes*, [Lecture notes] Accessed 14-6-21, [https://solidstate.quantumtinkerer.tudelft.nl/10\\_xray/#diffraction](https://solidstate.quantumtinkerer.tudelft.nl/10_xray/#diffraction).

- [13] S. H. Simon, *The Oxford Solid State Basics* (Oxford University Press, 2013) Chap. 14.
- [14] B. Henke, E. Gullikson, and J. Davis, *X-ray interactions: photoabsorption, scattering, transmission, and reflection at E=50-30000 eV, Z=1-92*, *Atomic Data and Nuclear Data Tables* **54**, 181 (1993).
- [15] Matt Hughes, SEMICORE Equipment Inc, *What is DC Sputtering?* **Accessed 19-6-21**, <http://www.semicore.com/news/94>.
- [16] Thin Film Consulting, *Fundamentals of sputtering, physical vapor deposition - pvd*, **Accessed 14-6-21**, <http://www.thfc.de/fundamentals>.
- [17] G. Chen, S. Chen, S. Huang, and H. Lee, *Growth mechanism of sputter deposited Ta and Ta-N thin films induced by an underlying titanium layer and varying nitrogen flow rates*, *Applied Surface Science* **169-170**, 353 (2001).
- [18] M. Newville, T. Stensitzki, D. B. Allen, and A. Ingargiola, *LMFIT: Non-Linear Least-Square Minimization and Curve-Fitting for Python*, (2014).
- [19] S. A. Speakman, *Basics of x-ray powder diffraction*, MIT Center for Materials Science and Engineering, [Powerpoint Slides] **Accessed 14-6-21**, <http://prism.mit.edu/xray/Basics%20of%20X> () .
- [20] S. A. Speakman, *Introduction to high resolution x-ray diffraction of epitaxial thin films*, MIT Center for Materials Science and Engineering, [Powerpoint Slides] **Accessed 14-6-21**, [http://prism.mit.edu/xray/oldsite/Introduction to HRXRD.pdf](http://prism.mit.edu/xray/oldsite/Introduction%20to%20HRXRD.pdf) () .
- [21] M. Björck and G. Andersson, *Genx: an extensible x-ray reflectivity refinement program utilizing differential evolution*, *Journal of Applied Crystallography* **40**, 1174 (2007).
- [22] R. Coloma Ribera, *Growth and thermal oxidation of Ru and ZrO<sub>2</sub> thin films as oxidation protective layers*, *Ph.D. thesis*, University of Twente (2017).
- [23] L. Bannenberg and H. Schreuders, *Hydrogenation kinetics of metal hydride catalytic layers*, (2021), [arXiv:2104.11703](https://arxiv.org/abs/2104.11703) [[cond-mat.mtrl-sci](https://arxiv.org/abs/2104.11703)] .
- [24] F. Manchester, A. San-Martin, and J. Pitre, *The H-Pd (hydrogen-palladium) System*, *Journal of Phase Equilibria* **31**, 62 (1994).
- [25] G. Pivak, H. Schreuders, M. Slaman, R. Griessen, and B. Dam, *Thermodynamics, stress release and hysteresis behavior in highly adhesive Pd-H films*, *International Journal of Hydrogen Energy* **36**, 4056 (2011).